Research Article Vol. 39, No. 4 / April 2022 / Journal of the Optical Society of America A 759

Journal of the Optical Society of America A

OPTICS, IMAGE SCIENCE, AND VISION

Speckle-based deep learning approach for classification of orbital angular momentum modes

Venugopal Raskatla,[1] B. P. Singh,[1] Satyajeet Patil,[2] Vijay Kumar,[1,*] and R. P. Singh[2]

[1]Department of Physics, National Institute of Technology Warangal, Warangal, Telangana 506004, India
[2]Physical Research Laboratory, Ahmedabad, Gujarat 380009, India
*Corresponding author: vijay@nitw.ac.in

Received 20 October 2021; revised 6 March 2022; accepted 8 March 2022; posted 8 March 2022; published 1 April 2022

We present a speckle-based deep learning approach for orbital angular momentum (OAM) mode classification. In this method, we have simulated the speckle fields of the Laguerre–Gauss (LG), Hermite–Gauss (HG), and superposition modes by multiplying these modes with a random phase function and then taking the Fourier transform. The intensity images of these speckle fields are fed to a convolutional neural network (CNN) for training a classification model that classifies modes with an accuracy >99%. We have trained and tested our method against the influence of atmospheric turbulence by training the models with perturbed LG, HG, and superposition modes and found that models are still able to classify modes with an accuracy >98%. We have also trained and tested our model with experimental speckle images of LG modes generated by three different ground glasses. We have achieved a maximum accuracy of 96% for the most robust case, where the model is trained with all simulated and experimental data. The novelty of the technique is that one can do the mode classification just by using a small portion of the speckle fields because speckle grains contain the information about the original mode, thus eliminating the need for capturing the whole modal field, which is modal dependent.

https://doi.org/10.1364/JOSAA.446352

1. INTRODUCTION

Beams having orbital angular momentum (OAM) have been a subject of interest for the past few decades. These beams possess an extra degree of freedom, which lends itself well to application in communication for increasing bandwidth and information-carrying capacity [1–4]. Apart from communication, they can be found in applications such as optical trapping [5,6], microscopy and imaging [7], quantum entanglement [8], and quantum information processing. They have a helical phase front with an azimuthal phase term $\exp(il\phi)$, where l is the topological charge and ϕ is the azimuthal angle. These beams have an OAM of $l\hbar$ per photon. Depending on the topological charge, the beam has different twisted wavefronts and can be quantified as optical modes. These modes have orthogonality properties while propagating coaxially. In general, any beam having a helical phase structure can be referred to as an OAM beam irrespective of its radial distribution. The paraxial solution of the wave equation in a cylindrical coordinate system and homogeneous media is a family of Laguerre–Gaussian (LG) beams that possess a vortex within them. These are a special subset of OAM beams whose azimuthal and radial wavefronts are well defined with two indices l and p, respectively. Here p refers to the radial nodes in the intensity profile [9].

One of the best ways for the generation and detection of the OAM modes is using a spatial light modulator (SLM) [10]. Generally, the interference and diffraction properties of the OAM modes are used to identify them [11,12]. However, these traditional methods for mode detection and demultiplexing are difficult to implement in real life. Mode detection using these methods requires a precise alignment of high-quality optical components to get the exact mode information. The machine learning and deep learning approaches are being proposed and demonstrated to reduce the complexity and increase the accuracy of the system for OAM mode demultiplexing [2,4,13–19]. The power of deep learning, specifically convolutional neural networks (CNNs), is utilized by using both direct OAM intensity images and interferograms [20,21]. Various CNN architectures and joint algorithms are being proposed to efficiently classify OAM modes [22–25]. Although these methods reduce the complexity and increase the accuracy of demultiplexing, they are noise limited. The accuracy of mode classification depends on the amount of distortion and noise introduced in the input beam. In practice, when these models are deployed for demultiplexing in free-space communication systems, due to atmospheric turbulence, the modes get distorted and become difficult to detect. Moreover, these techniques require capturing

the full image of the mode for accurate classification. But capturing the full modal image may not be feasible since mode size increases with the azimuthal (l) and radial (p) indices.

In this paper, we propose a speckle-based deep learning approach [26,27] to address these issues. We have modified Alexnet, a pretrained neural network for building a deep learning based classification model. Using the pretrained network is a much faster and more efficient way to train the model than building from scratch. It also reduces the need for a large amount of data, as it has already learned a lot of features. Speckle intensity patterns of Hermite–Gauss (HG), LG, and superposition modes generated by multiplying with random phase function are used as the input to this neural network. The advantage of using a speckle pattern is to eliminate the need of capturing the large full modal image. Using the proposed technique, the OAM mode can be recognized just by using a small portion of the speckle pattern. To test the generality, we have trained and tested the model for speckle images generated by different random phase functions and for experimental images of LG modes generated by different round glasses (GG). To test the robustness, we have also trained and tested for the modes perturbed due to atmospheric turbulence. This paper demonstrates the fundamental proof of concept of the proposed novel technique, which is an add-on to the previously existing machine-learning-based OAM demultiplexers.

2. OAM AND SUPERPOSITION MODES

The OAM modes are the solutions of a free-space paraxial wave equation that has different solutions in different coordinate systems. For example, the HG beams are the solution in the Cartesian coordinate system, whereas the family of LG beams carrying optical vortices are the solutions in the cylindrical coordinate system.

The expression for HG modes is given as

$$\begin{aligned}&\mathrm{HG}_{m,n}(\boldsymbol{x},\boldsymbol{y},\boldsymbol{z})\\&=A_0\left(\frac{w_0}{w(z)}\right)H_m\left(\frac{\sqrt{2}x}{w(z)}\right)H_n\left(\frac{\sqrt{2}y}{w(z)}\right)\exp\left(-\frac{x^2+y^2}{w(z)^2}\right)\\&\times\exp\left[-ikz-ik\frac{(x^2+y^2)}{2}+i(m+n+1)\Phi(z)\right],\end{aligned}\tag{1}$$

where A_0 is amplitude, $R(z)=z+z_0^2/z$ is the wavefront curvature of the beam, $w(z)=w_0\sqrt{1+z^2/z_0^2}$ is the effective width of the beam, $\Phi(z)=\arctan(z/z_0)$ is the Gouy phase shift, $z_0=\pi w_0^2/\lambda$ is the Rayleigh range, and H_m and H_n are Hermite polynomials of order m and n, respectively. Here m and n are positive integers and represent the number of nodes along x and y axis.

Similarly, the expression for LG beams is given as

$$\begin{aligned}&\mathrm{LG}_{p,l}(\rho,\phi,z)\\&=A_0\left(\frac{w_0}{w(z)}\right)\left(\frac{\rho}{w(z)}\right)^{|l|}L_p^{|l|}\left(\frac{2\rho^2}{w^2(z)}\right)\exp\left(-\frac{\rho^2}{w(z)^2}\right)\\&\times\exp\left[-ikz-ik\frac{\rho^2}{2R(z)}-il\phi+i(|l|+2p+1)\Phi(z)\right],\end{aligned}\tag{2}$$

where p is nonnegative integer, l is an integer, and $L_p^{|l|}$ is an associated Laguerre function of order p and l. Here p is termed as the radial mode index and l as the azimuthal mode index.

The superposition of LG modes for $l=1-16$ is given as [2]

$$\mathrm{SM}_{-l,l}=\mathrm{LG}_{0,-l}+\mathrm{LG}_{0,l}.\tag{3}$$

3. GENERATION OF OAM SPECKLE FIELD

A. Simulation

We have simulated speckle field for Eqs. (1)–(3) in MATLAB 2021a. For generating the speckles, we have multiplied the field with random phase functions having uniformly distributed random phase values between 0 and 2π and have taken its Fourier transform. Mathematically, this can be expressed as

$$u_{\mathrm{sc}}(\boldsymbol{r})=\mathcal{F}\{u(\boldsymbol{r})e^{i\phi_{R_i}(r)}\}.\tag{4}$$

Here, $u(\boldsymbol{r})$ takes $\mathrm{HG}_{m,n}/\mathrm{LG}_{p,l}/\mathrm{SM}_{-l,l}$, $\mathcal{F}$ denotes the Fourier transform, and $\phi_{R_i}(\boldsymbol{r})$ corresponds to the random phase. The intensity distribution of the speckle field is then calculated as

$$I_{\mathrm{sc}}(\boldsymbol{r})=u_{\mathrm{sc}}(\boldsymbol{r})u_{sc}^{*}(\boldsymbol{r}).\tag{5}$$

By varying the phase distribution in the phase function, different speckle images are simulated. We have generated three different datasets for three different phase functions [$\{\phi_{R_1}\}$, $\{\phi_{R_2}\}$, $\{\phi_{R_3}\}$], each analogous to different ground glass. In each phase function, the unit of the random phase is of the order of 2^a pixels, where $a=0,1,2$. The LG dataset has eight different $\mathrm{LG}_{p,l}$ modes with $p=0$ and $l=1-8$, the HG dataset contains 36 different $\mathrm{HG}_{m,n}$ modes with $m,n=0-5$, and the $\mathrm{SM}_{-l,l}$ dataset has 16 different superposition modes with $l=1-16$. Each dataset includes 1000 images of each class.

The atmospheric turbulence effects on the modes are incorporated by turbulence phase screens using the modified atmospheric spectrum model [28]. The equivalent phase is given by the following expression:

$$\begin{aligned}\Phi_n(\kappa)&=0.033C_n^2\left[1+1.802\left(\frac{\kappa}{\kappa_l}\right)-0.254\left(\frac{\kappa}{\kappa_l}\right)^{\frac{7}{6}}\right]\\&\times\exp\left(-\frac{\kappa^2}{\kappa_l^2}\right)(\kappa^2+\kappa_0^2)^{-\frac{11}{6}}.\end{aligned}\tag{6}$$

Here, C_n^2 is the refractive index structure parameter indicating the turbulence strength, $k_l=3.3/l_0$, $k_0=2\pi/L_0$, and l_0 and L_0 are the internal and external scales, respectively.

Figure 1(a) illustrates the simulation results for the speckles of the LG, HG, and superposition modes through three different random phase functions. Figure 1(b) shows the influence of the turbulence phase screen on the original modes and their corresponding speckle distribution. A small region from each speckle images is fed to the CNN for training and testing the classification model as shown in Fig. 1(c).

B. Experiment

Figure 2 shows the experimental schematic for generating and capturing the speckle field of LG modes in the far-field region.

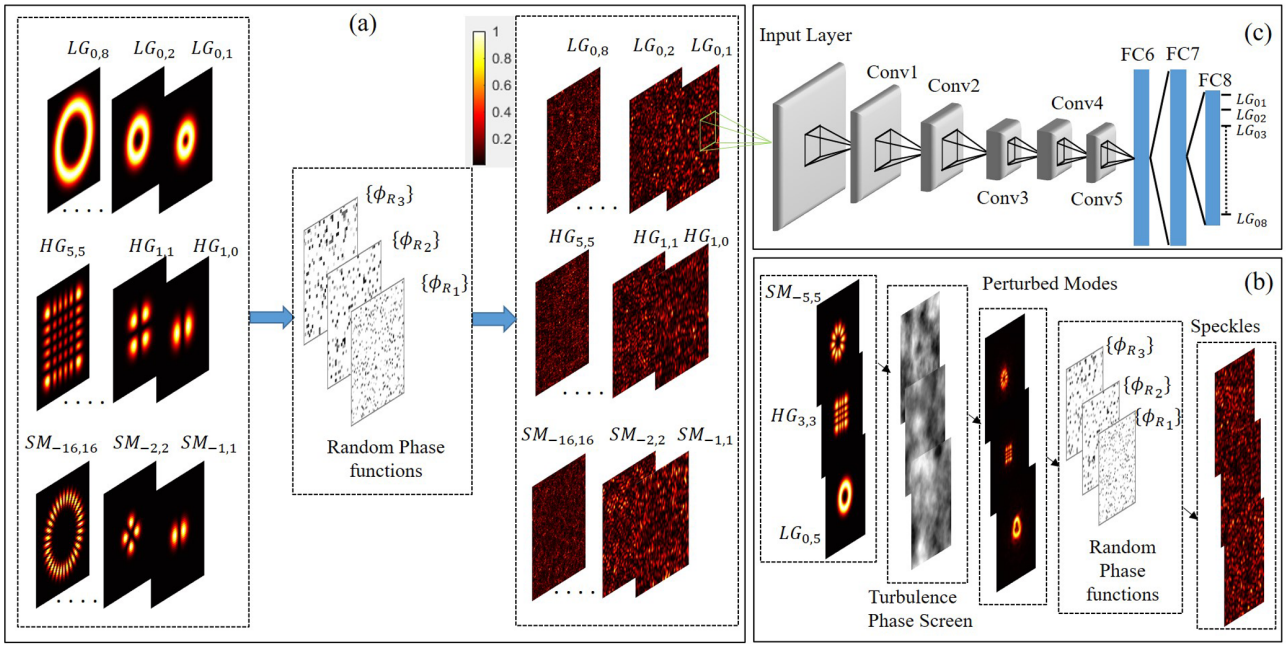

Fig. 1. Simulation results for (a) LG, HG, and superposition modes and their corresponding speckles distribution for three different sets of random phase functions; (b) turbulence phase screen and its manifestation on modes. (c) Modified Alexnet for training and testing the classification model.

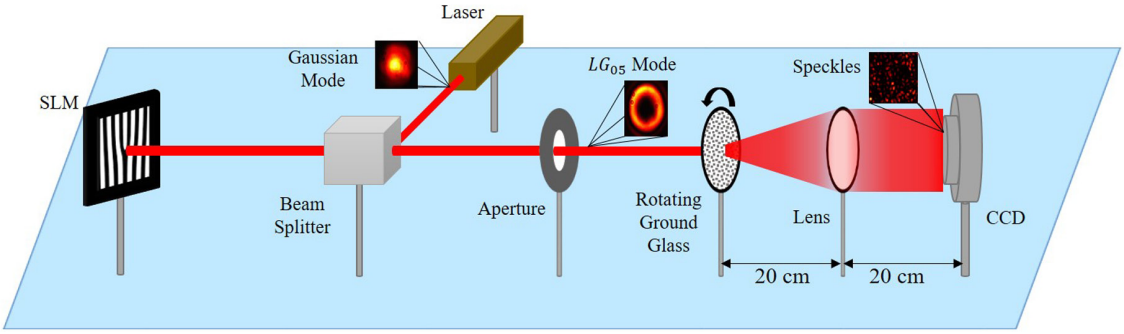

Fig. 2. Schematic of the experimental setup for the speckle-based deep learning approach for OAM mode classification.

A spatial light modulator (SLM) displaying a binary phase hologram is illuminated by a linearly polarized 5 mW He–Ne laser beam. Along with the desired mode, various higher-order modes are also generated, and an aperture is used for isolating the desired LG mode. Ground glass with grit 120 (GG120) (DG10-120, Thorlab) that acts as a random phase mask is placed in the path of the LG modes at the back focal plane of the converging lens. The far-field speckle intensity patterns of the LG modes with $l = 1 - 8$ and $p = 0$ are captured by a CCD camera (Spiricon SP620U) with a resolution of 1600 × 1200 pixels and pixel spacing of 4 μm × 4 μm placed at the front focal plane of the lens. By rotating the ground glass in the vertical plane and thus exposing the input beam to different random phase profiles, we have captured 1200 speckle images for each mode. We have repeated the experiment to generate 1200 speckle images of each LG mode for ground glass grit 600 (GG600) (DG10-600, Thorlab) and 1500 (GG1500) (DG10-1500, Thorlab).

Since every region of the speckle pattern contains information about the input mode, instead of using a full image, we have randomly selected a region of 512 × 512 pixels (image size lower than 512 × 512 will lead to lower modal classification accuracy) from each image and generated a dataset for training and testing our model. Thus, we have three experimental datasets, each having 1200 speckle images of $\mathrm{LG}_{p,l}$ modes with $p = 0$ and $l = 1-8$. The intention of randomly selecting a smaller region of the complete speckle pattern is to demonstrate the fact that a small portion of the speckle field will be enough for modal classification and thus reduce the computational load. Additionally, it also demonstrates the non-line-of-sight communication.

During the experiment, the ground glass position (x, y) is taken into account, as we are generating different speckle images by rotating the ground glass in a transverse plane. Since we are capturing the speckles in the Fourier plane, the diffusor's position (z) relative to the camera and lens is an important experimental parameter. Experimentally, it is very difficult to rotate the ground glass in the exact transverse plane, and thus the

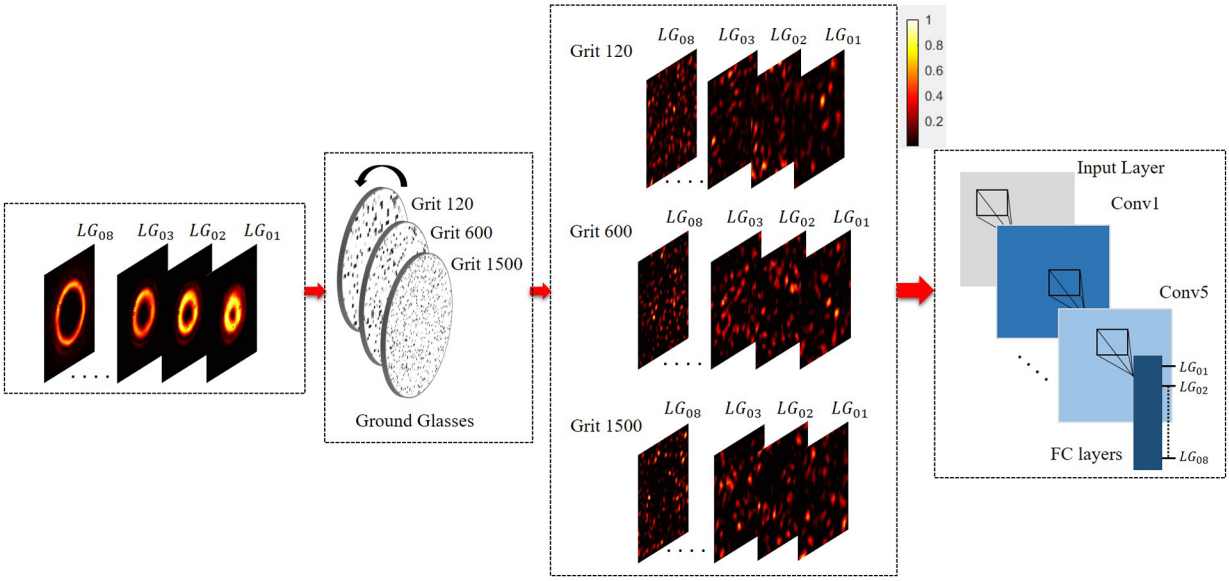

Fig. 3. Experimental results for eight different $LG_{p,l}$ modes and their corresponding speckles generated from rotating ground glasses of grit 120, 600, and 1500. The speckle images are fed to the CNN network to train and test the classification model.

experimental parameters, such as angles (roll, yaw, pitch), are also included in the experimentally generated dataset. Figure 3 illustrates the experimentally generated $LG_{p,l}$ modes and corresponding speckle images generated by passing them through three different ground glasses. The speckle grain size ranges from 30 to 16 pixels, 36 to 16 pixels, and 40 to 16 pixels for GG120, GG600, and GG1500, respectively.

4. DEEP LEARNING MODEL FOR OAM MODE CLASSIFICATION

Inspired by the human brain, a CNN is a deep neural network composed of multiple layers of artificial neurons. The layers in a CNN include convolution layers, nonlinearity layers, pooling layers, and fully connected layers. When the image propagates through these layers, abstract features of the input image are obtained. The first layer extracts the simple features, whereas deeper layers extract higher-level features. Mathematically, as the convolution is dot product multiplication of two sets of elements, the features are self-learned by the CNN network through several convolution operations between the filters and images when passed through different convolution layers. Each layer is associated with different filters, and therefore different features can be extracted at different layers [29]. These filters are convolved with the input image and activate a certain feature of the image.

By adding pooling layers, nonlinear downsampling is performed to reduce the parameters that the network needs to learn as the pooling operation involves sliding a two-dimensional filter over each kernel of a feature map and summarizing the features lying within the region covered by the filter. Activation functions such as the rectified linear unit (ReLU) help in faster and more effective training by maintaining the positive values and mapping negative values to zero. After several convolutional, nonlinear, and pooling layers, all the features learned are combined by a fully connected layer to identify larger patterns. The output layers consist of softmax and classification layers (for classification purposes). The softmax layer applies the softmax function to the input and gives a normalized output, which is then converted to output classes by the classification layer that we wish to classify. For our scheme, we use such a pretrained network Alexnet, which is trained over a million images for 1000 classes. It has five convolutional layers and three fully connected layers. A softmax function is operated on the last fully connected layer, which gives the prediction of the label in terms of probabilities. Alexnet is well known for its simple

Table 1. Alexnet Architecture Modified for Training LG, HG, and Superposition Modes

Layer Name	No. of Filters	Filter Size	Stride	Padding	Size of Feature Map	Activation Function
data	—	—	—	—	227 × 227 × 3	—
conv1	96	11 × 11	4	—	55 × 55 × 96	MP + ReLu
conv2	256	5 × 5	1	2	27 × 27 × 256	MP + ReLu
conv3	384	3 × 3	1	1	13 × 13 × 384	ReLu
conv4	384	3 × 3	1	1	13 × 13 × 384	ReLu
conv5	256	3 × 3	1	1	13 × 13 × 256	MP + ReLu
fc6	4096	—	—	—	1 × 1 × 4096	ReLU + Dropout
fc7	4096	—	—	—	1 × 1 × 4096	ReLU + Dropout
fc8	8/36/16	—	—	—	1 × 1 × 8/32/16	Softmax

architecture, moderate computational speed, and high accuracy. The details of the Alexnet architecture are presented in Table 1.

We have modified the last layer of Alexnet to classify OAM modes and superposition (8 for LG, 32 for HG, and 16 for superposition modes). Use of the pretrained network is a much faster and more efficient way to train the model than building from scratch. It also reduces the need for a large amount of data, as it has already learned a lot of features. We have preprocessed our data before feeding it to the network, as the input layer of Alexnet only accepts images of the size $227 \times 227 \times 3$. We have trained and tested the network separately for all three types of modes using simulation images. In addition, we also have trained and tested the network for LG modes using experimental images. For more robustness, we have also trained the LG classification model for all datasets collectively (simulation + experiment). In each case, 80% images of the dataset are used for training, and the remaining 20% are used for testing. The network is trained using the Stochastic Gradient Decent with Momentum algorithm with a constant learning rate of 0.0001 and momentum 0.9 on a single i7 9700 CPU with 32 GB RAM in MATLAB 2021a.

5. RESULTS AND ANALYSIS

Table 2 shows the classification accuracies for the model trained with simulated and experimental images of LG modes. We have achieved an accuracy of >99% for the HG and superposition modes' classification models trained on an individual dataset as well as for a cumulative dataset.

Table 2. Classification Accuracies for LG Mode Classification Models Trained on Different Datasets

Data Used for Training	Accuracy
$\{\phi_{R_1}\}$	>99%
$\{\phi_{R_2}\}$	>99%
$\{\phi_{R_3}\}$	>99%
$\{\phi_{R_1}\} + \{\phi_{R_2}\} + \{\phi_{R_3}\}$	99%
$GG120$	92%
$GG600$	94%
$GG1500$	94%
$GG120 + GG600 + GG1500$	96%

To test the generality of our technique, we have tested the data generated by one ground glass on the network trained using the data generated by others. The Table 3 shows the classification accuracy for each combination. To increase the generality of our model, we have first trained the network using data generated by two ground glasses and tested the data generated by a third one. As shown in Table 3, the accuracy is improved significantly. So for a more general model, the training should be done on the cumulative data generated by different ground glasses.

Figure 4(a) shows the training progress of the LG classification model trained for all datasets collectively (simulation + experiment) to make the model more general. The accuracy (blue curve) and loss (orange curve) are plotted against the iterations during training. In the beginning, the training starts by assignment of random weights and biases (learning parameters), resulting in less accuracy and high loss. As the training

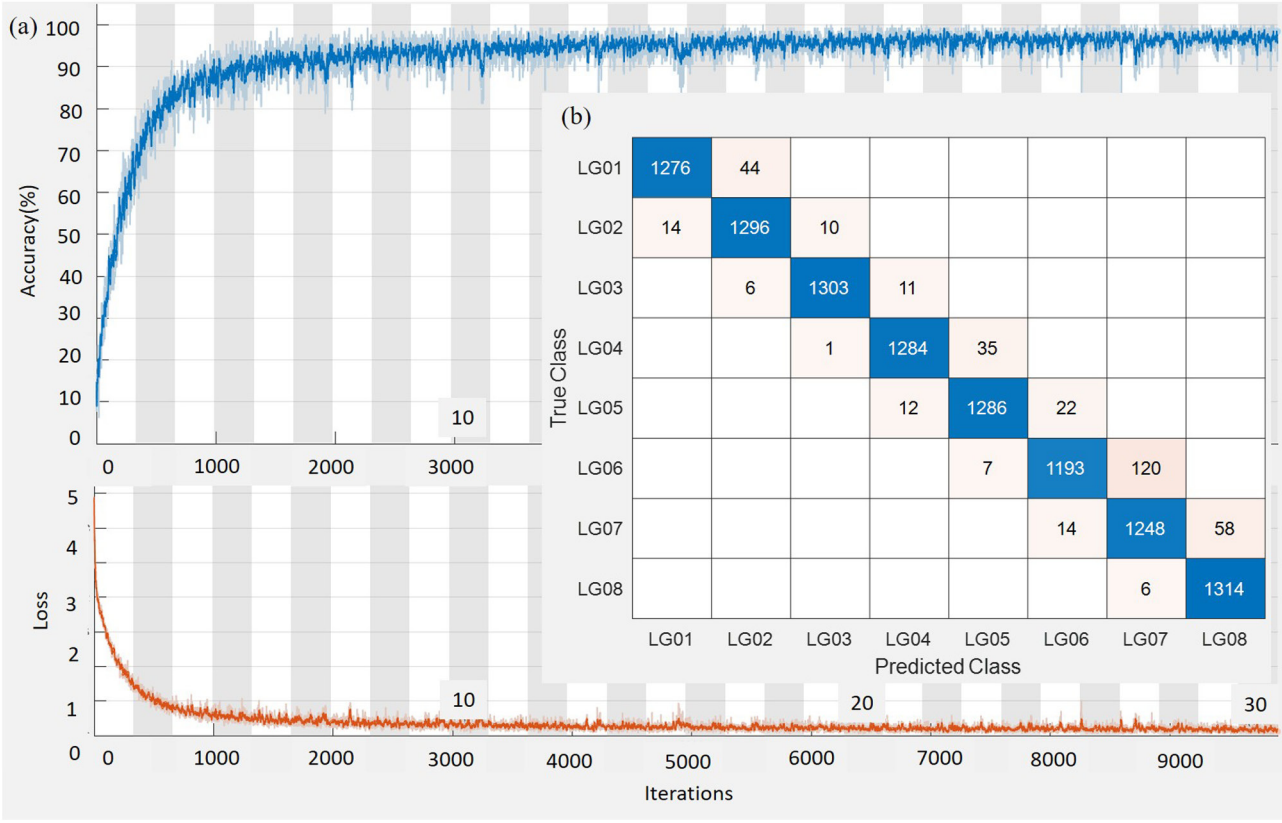

Fig. 4. (a) Training progress with accuracy and loss plotted against iterations during the training of the LG classification model for a cumulative dataset of experiment and simulation. (b) Confusion matrix indicating misclassification.

Table 3. Classification Accuracies of Different Trained Models to Test Generality

Data Used for Training	Data Used for Testing	Accuracy
$GG120$	$GG600$	41%
$GG120$	$GG1500$	54%
$GG600$	$GG120$	14%
$GG600$	$GG1500$	87%
$GG1500$	$GG120$	25%
$GG1500$	$GG600$	78%
$GG120 + GG600$	$GG1500$	89%
$GG120 + GG1500$	$GG600$	92%
$GG600 + GG1500$	$GG120$	48%

progresses, the weights and biases are adjusted using the back-propagation algorithm so that loss is reduced and reaches zero, whereas the accuracy of classification reaches the maximum value. Figure 4(b) shows the confusion matrix for the same case, indicating the prediction of OAM modes with an accuracy of $>96\%$.

To test the robustness and the influence of atmospheric turbulence, we have trained and tested our model using simulated speckle images of perturbed LG, HG, and superposition modes. The perturbation is introduced by passing these modes through a turbulence phase screen generated by Eq. (6) with $C_n^2 = 1 \times 10^{-14}\ \mathrm{m}^{-2/3}$, $l_0 = 1$ cm, and $L_0 = 100$ m as shown in Fig. 1(b). We have achieved an accuracy $>98\%$ for each types of mode (LG, HG, SM) and found that distortion introduced by turbulence (that will affect the modal energy distribution at the detector) will not affect the classification accuracy, if it is included in the training itself. Our results show that the CNN network is learning the underlying distribution of OAM modes but more robustness and generality the network should be trained with a variety of data for learning maximum features.

6. SUMMARY AND CONCLUSION

We have presented a novel approach for classification of OAM and superposition modes based on speckle patterns and deep learning. To train the classification model, the last layer of Alexnet is modified to classify 8 LG, 36 HG, and 16 superposition modes. These modes are multiplied with different random phase functions to simulate the speckle field. The speckle images generated are then used for training and testing the model. The LG mode classification model is also trained and tested on experimental images generated by different ground glasses. To make our model more general, we have trained it on a cumulative dataset by including all the images generated by different ground glasses and random phase functions. We have also trained our model by including the atmospheric turbulence effect by multiplying the modes with turbulence phase screens. Our technique stands out as different than previous studies because, in contrast to feeding the full direct OAM mode images to a deep learning model for classification, a small region randomly selected from the speckle patterns of the respective OAM modes is used. The main advantage of our methodology is that a portion of the captured field having a sufficient number of speckle grains is sufficient for mode identification. Our study shows that these modes need not be pure, and this technique can also be used for noisy modes. Thus, we believe that our approach is noise and alignment independent, and it has the capability to be deployed for demultiplexing the OAM modes for line-of-sight as well as non-line-of-sight free-space optical communication. It will increase the fidelity and accuracy of demultiplexing along with the speed of the system. We have modified and implemented a pretrained network that reduces the computational load (i.e., it requires a smaller number of images for training) and power for training compared to the network trained from the scratch. Hence, it can be easily implementable in any standard computer without a GPU.

Funding. Science and Engineering Research Board (SRG/2021/001375); NITW RSM grant (P1138).

Acknowledgment. V. K. acknowledges SERB and NITW RSM.

Disclosures. The authors declare no conflicts of interest.

Data availability. Data underlying the results presented in this paper are available upon reasonable request from the authors.

REFERENCES

1. J. Wang, J.-Y. Yang, I. M. Fazal, N. Ahmed, Y. Yan, H. Huang, Y. Ren, Y. Yue, S. Dolinar, M. Tur, and A. E. Willner, "Terabit free-space data transmission employing orbital angular momentum multiplexing," Nat. Photonics **6**, 488–496 (2012).
2. M. Krenn, R. Fickler, M. Fink, J. Handsteiner, M. Malik, T. Scheidl, R. Ursin, and A. Zeilinger, "Communication with spatially modulated light through turbulent air across Vienna," New J. Phys. **16**, 113028 (2014).
3. M. Krenn, J. Handsteiner, M. Fink, R. Fickler, R. Ursin, M. Malik, and A. Zeilinger, "Twisted light transmission over 143 km," Proc. Natl. Acad. Sci. USA **113**, 13648–13653 (2016).
4. Z. Liu, Y. Huang, H. Liu, and X. Chen, "Non-line-of-sight optical communication based on orbital angular momentum," Opt. Lett. **46**, 5112–5115 (2021).
5. K. Dholakia, M. MacDonald, and G. Spalding, "Optical tweezers: the next generation," Phys. World **15**, 31–35 (2002).
6. D. G. Grier, "A revolution in optical manipulation," Nature **424**, 810–816 (2003).
7. S. Fürhapter, A. Jesacher, S. Bernet, and M. Ritsch-Marte, "Spiral phase contrast imaging in microscopy," Opt. Express **13**, 689–694 (2005).
8. A. Mair, A. Vaziri, G. Weihs, and A. Zeilinger, "Entanglement of the orbital angular momentum states of photons," Nature **412**, 313–316 (2001).
9. A. E. Willner, H. Huang, Y. Yan, Y. Ren, N. Ahmed, G. Xie, C. Bao, L. Li, Y. Cao, Z. Zhao, J. Wang, M. P. J. Lavery, M. Tur, S. Ramachandran, A. F. Molisch, N. Ashrafi, and S. Ashrafi, "Optical communications using orbital angular momentum beams," Adv. Opt. Photon. **7**, 66–106 (2015).
10. A. Forbes, A. Dudley, and M. McLaren, "Creation and detection of optical modes with spatial light modulators," Adv. Opt. Photon. **8**, 200–227 (2016).
11. Y. Shen, X. Wang, Z. Xie, C. Min, X. Fu, Q. Liu, M. Gong, and X. Yuan, "Optical vortices 30 years on: OAM manipulation from topological charge to multiple singularities," Light Sci. Appl. **8**, 90 (2019).
12. Y. Bai, H. Lv, X. Fu, and Y. Yang, "Vortex beam: generation and detection of orbital angular momentum [Invited]," Chin. Opt. Lett. **20**, 012601 (2022).
13. T. Doster and A. T. Watnik, "Machine learning approach to OAM beam demultiplexing via convolutional neural networks," Appl. Opt. **56**, 3386–3396 (2017).
14. J. Delpiano, G. L. Funes, J. E. Cisternas, S. Galaz, and J. A. Anguita, "Deep learning for image-based classification of OAM modes in

laser beams propagating through convective turbulence," Proc. SPIE **11133**, 1113305 (2019).
15. S. Sharifi, Y. Banadaki, G. Veronis, and J. P. Dowling, "Towards classification of experimental Laguerre–Gaussian modes using convolutional neural networks," Opt. Eng. **59**, 076113 (2020).
16. A. Bekerman, S. Froim, B. Hadad, and A. Bahabad, "Beam profiler network (BPNet): a deep learning approach to mode demultiplexing of Laguerre–Gaussian optical beams," Opt. Lett. **44**, 3629–3632 (2019).
17. W. Xiong, Y. Luo, J. Liu, Z. Huang, P. Wang, G. Zhao, Y. Li, Y. Gao, S. Chen, and D. Fan, "Convolutional neural network assisted optical orbital angular momentum identification of vortex beams," IEEE Access **8**, 193801 (2020).
18. L. R. Hofer, L. W. Jones, J. L. Goedert, and R. V. Dragone, "Hermite–Gaussian mode detection via convolution neural networks," J. Opt. Soc. Am. A **36**, 936–943 (2019).
19. Y. An, T. Hou, J. Li, L. Huang, J. Leng, L. Yang, and P. Zhou, "Fast modal analysis for Hermite–Gaussian beams via deep learning," Appl. Opt. **59**, 1954–1959 (2020).
20. X. Fu, Y. Bai, and Y. Yang, "Measuring OAM by the hybrid scheme of interference and convolutional neural network," Opt. Eng. **60**, 064109 (2021).
21. M. A. Cox, T. Celik, Y. Genga, and A. V. Drozdov, "Interferometric orbital angular momentum mode detection in turbulence with deep learning," Appl. Opt. **61**, D1–D6 (2022).
22. S. Lohani, E. M. Knutson, M. O'Donnell, S. D. Huver, and R. T. Glasser, "On the use of deep neural networks in optical communications," Appl. Opt. **57**, 4180–4190 (2018).
23. J. Li, M. Zhang, and D. Wang, "Adaptive demodulator using machine learning for orbital angular momentum shift keying," IEEE Photon. Technol. Lett. **29**, 1455–1458 (2017).
24. Z. Wang, M. I. Dedo, K. Guo, K. Zhou, F. Shen, Y. Sun, S. Liu, and Z. Guo, "Efficient recognition of the propagated orbital angular momentum modes in turbulences with the convolutional neural network," IEEE Photon. J. **11**, 7903614 (2019).
25. Q. Zhao, S. Hao, Y. Wang, L. Wang, X. Wan, and C. Xu, "Mode detection of misaligned orbital angular momentum beams based on convolutional neural network," Appl. Opt. **57**, 10152–10158 (2018).
26. V. Raskatla and V. Kumar, "Deep learning assisted OAM modes demultiplexing," Proc. SPIE **12126**, 121260A (2021).
27. V. Raskatla and V. Kumar, "Deep learning assisted classification of noisy Laguerre Gaussian modes," in *Frontiers in Optics/Laser Science* (Optica, 2021), paper JTu1A.16.
28. L. C. Andrews and R. L. Phillips, *Laser Beam Propagation through Random Media*, 2nd ed., Vol. **152** of SPIE Press Monograph (SPIE Press, 2005).
29. S. Albawi, T. A. Mohammed, and S. Al-Zawi, "Understanding of a convolutional neural network," in *International Conference on Engineering and Technology (ICET)* (IEEE, 2017), pp. 1–6.